Chemical Physics Letters 713 (2018) 91–97

Contents lists available at ScienceDirect

Chemical Physics Letters

journal homepage: www.elsevier.com/locate/cplett

Comment

# Architectured mesoporous materials modified with nickel for alternative energy and environmental applications: Hydrogen storage and photo-Fenton contaminant degradation

P.M. Carraro[a,b], T.B. Benzaquén[a], M.I. Oliva[b], G.A. Eimer[a,*]

[a] CITeQ – CONICET – UTN, Universidad Tecnológica Nacional – Facultad Regional Córdoba, Córdoba, Argentina
[b] IFEG – CONICET – UNC, Universidad Nacional de Córdoba, Córdoba, Argentina

## HIGHLIGHTS

- The synthesis time influences on the textural and chemical properties of Ni-MCM-41.
- Ni incorporation into mesoporous walls decreases the accessibility to the active sites.
- The low Ni loading favor the $H_2$ adsorption of Ni-MCM-41 materials at 77 K.
- Ni-MCM-41 materials provided an interest alternative in Atrazine degradation.

## ARTICLE INFO

*Keywords:*
MCM-41
Nickel
Hydrogen storage
Atrazine degradation

## ABSTRACT

Ni-MCM-41 nanocomposites were prepared by direct hydrothermal synthesis with different Ni contents. Various characterization techniques were conducted in order to study the properties of the materials. $H_2$ storage capacity and degradation of atrazine by heterogeneous photo-Fenton-like process were studied. The results indicated that the structural, chemical, adsorption and catalytic properties of the resulting materials strongly depend on the hydrothermal treatment days and the nickel content. The increase in the Si/Ni molar ratio leads to higher presence of nickel oxide and increment in hydrothermal treatment days favours the Ni incorporation inside mesoporous walls, decreasing the accessibility to the active sites.

## 1. Introduction

Environmental pollution is one of the greatest problems that the human civilization is facing today. Industrial and agricultural activities generate serious environmental pollution in air, water and soil, deteriorating the ecological balance of ecosystems and the human health. On the one hand, the massive energy demand of the world is mainly satisfied by the nonrenewable fossil fuels, which produce environmental pollution problems and undesired alterations in the weather patterns arising from global warming effect. The decrease of fossil fuel supply and global warming require the search of new alternative and renewable energy sources [1]. Hydrogen is regarded as a future energy carrier due to its high energy density per unit as long as it is produced from renewable sources. However, the on-board vehicular hydrogen storage is the main barrier for the implementation of hydrogen economy. Therefore, many studies are focused on nanoporous materials as hydrogen storage systems, which must meet the requirements established by D.O.E (United States Department of the Energy) [2–5].

On the other hand, the water pollution by toxic pollutants is other major concern today. Among different agrochemicals, atrazine is one of the most widely used herbicides in sugarcane, corn and sorghum cultures [6,7]. Due to the direct application of atrazine to crops, there is the opportunity for the substance to contaminate soil and, consequently, water sources via runoff. This pollutant, not readily biodegradable presents relatively high persistence [8]. Current research shows that atrazine exposure may pose a threat to human health, with drinking water providing the most widespread route of exposure [9]. In this sense, the called advanced oxidation processes (AOPs) are being investigated exhaustively for the removal of contaminants from the environment [10]. Among them, the photo-Fenton process appears as an effective alternative method to treat recalcitrant organic pollutants like most agrochemicals [11,12]. Besides Fe (conventional Fenton process), other transition metals can also catalyze the reaction mentioned above. In fact, the reaction system using Ni as the photo-Fenton

* Corresponding author.
*E-mail addresses:* pcarraro@frc.utn.edu.ar (P.M. Carraro), geimer@frc.utn.edu.ar (G.A. Eimer).

https://doi.org/10.1016/j.cplett.2018.10.036
Received 27 June 2018; Accepted 12 October 2018
Available online 12 October 2018
0009-2614/ 

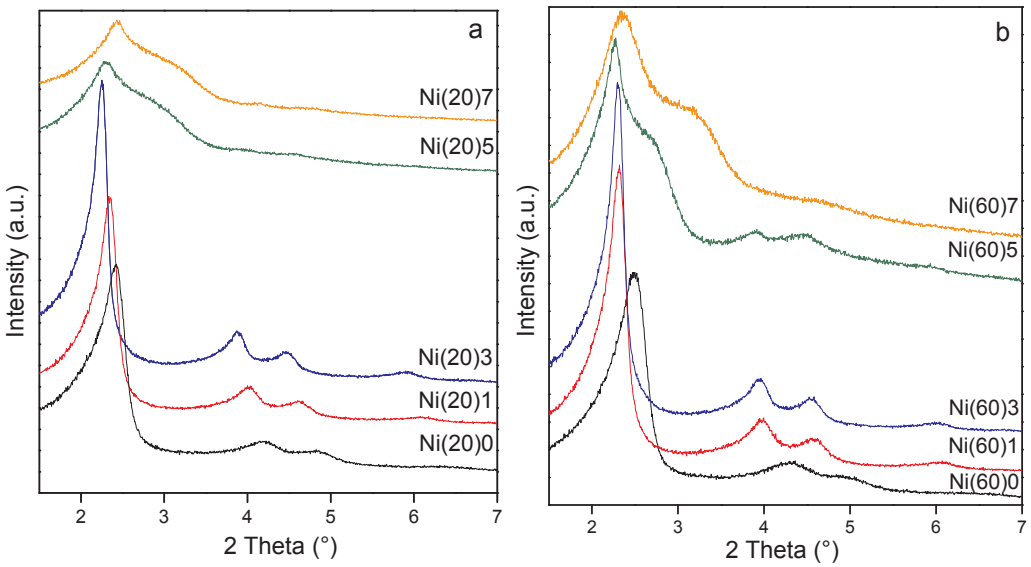


**Fig. 1.** Low-angle XRD patterns of samples with Si/Ni molar ratios (a) 20 and (b) 60.

catalyst can follow a similar "mechanism of reaction" as that of Fe and is referred as a photo-Fenton-like reaction [13–15]. Recently, much attention has been paid to the photo-Fenton and photo-Fenton-like processes, mainly focusing on the heterogeneous process [16]. Thus, the use of heterogeneous catalysts, such as mesoporous materials, provides an easy separation and recovery of the catalyst from the treated wastewater, not causing secondary metal ion pollution [17].

The discovery of the new family of mesoporous molecular sieves M41S in 1992 by Mobil scientists [18], opened a new area of inorganic nanoporous materials with very promising applications [18]. One of the members of this family, the MCM-41 materials have attracted much interest, mostly due to their large specific area ($> 900\ m^2/g$) and controlled pore dimensions with uniform pore size distribution (2–10 nm). Mesoporous materials modified with various heteroatoms into the framework, such as Fe, Ni, Pt, Pd, Cu, have received considerable attention in catalytic processes [19–22] as well as in adsorption processes. A number of synthesis methods have been studied to modify the MCM-41 support with an appropriate metallic cation, achieving a proper metal dispersion and improving the number of active sites per unit area [23–25]. Thus, in order to improve the hydrogen storage of these materials, it is well known that the metal incorporation into the pure siliceous MCM-41 structure increases the hydrogen adsorption capacity [25–27]. Incorporation of metals into the pores of mesoporous materials can be achieved by direct synthesis or by post-synthesis. The addition of the metal ions during the synthesis of the mesoporous materials can preferably lead to stabilization of highly dispersed metal species into the mesoporous framework. Meanwhile, post-synthesis methods such as wet impregnation, favor the formation of bigger metal oxides over the surface of support. In previous studies [26,28], we have reported that low Ni loadings favoured the hydrogen adsorption of MCM-41 materials modified with Ni by wet impregnation method. On the other hand, Parasanth et al. (2010), reported that metal incorporation into the mesoporous materials in situ during hydrothermal synthesis enhanced of hydrogen adsorption.

In this sense, MCM-41 modified with nickel by direct incorporation method, constitutes a very attractive solid in order to investigate the hydrogen adsorption as well as the degradation of pollutants in aqueous solution using Fenton and photo-Fenton systems.

In this work, we present the preparation of nickel modified mesoporous silica by a direct synthesis method based on a sol-gel process. The influence of the Si/Ni molar ratio in the synthesis gel and the hydrothermal treatment days on the physico-chemical properties has been studied. We focus on the study of the effect of nickel over the structural order, textural and chemical properties. Thus, mesoporous materials were exhaustively characterized to determine their potential utilization as materials for hydrogen storage and degradation of a model agrochemical (atrazine, ATZ) by a heterogeneous photo-Fenton process.

## 2. Materials and methods

### 2.1. Synthesis and characterization

The nickel-containing mesoporous materials were prepared by hydrothermal synthesis and the samples were named as Ni(*x*)y, where "*x*" is the Si/Ni initial molar ratio and "*y*" is the hydrothermal treatment days. See Supporting Information for details on synthesis procedure and different characterization techniques employed.

### 2.2. Hydrogen storage measurement

Hydrogen (99.999%) physisorption experiments at 77 K and pressures up to 10 bar were performed using an automated nanometric system ASAP 2050 (Micromeritics Instrument Corporation). Previous to all the adsorption experiments, the samples were degassed at 573 K during 12 h under vacuum conditions ($5 \times 10^{-3}$ mmHg).

### 2.3. Atrazine degradation

Photo-Fenton-like reactions for atrazine (ATZ, 2-chloro-4-ethylamino-6-isopropylamino-striazine, $C_8H_{14}ClN_5$, ≥90%, SYNGENTA) degradation were carried out in an isothermal, well mixed, batch annular reactor. See Supporting Information for details on the experimental reaction and atrazine concentration measured [29].

Supplementary information about the device, procedures and the degradation processes of this herbicide under photo-Fenton system can be found in Benzaquén et al. [30].

## 3. Results and discussion

### 3.1. Characterization of the solids

Fig. 1a and b show the XRD patterns obtained for all the calcined materials with initial Si/Ni molar ratios = 20 and 60 in the initial gel and synthesis days of 0, 1, 3, 5 and 7 days. All of the patterns exhibit a main (1 0 0) peak and three weak reflections ascribed to (1 1 0), (2 0 0) and (2 1 0) planes, which are typical of highly ordered MCM-41

structures. As it is known, the number of well-defined peaks and their relative intensities represent the relative structural ordering of MCM-41 materials [26]. Even though the mesostructure was formed before the hydrothermal treatment (0 days hydrothermal treatment), the structural ordering was increased when the samples were hydrothermally treated up to 3 days. Then, the decrease in the intensity of the first peak for the Ni(20,60)5 and Ni(20,60)7 samples, besides an evident broadening for all peaks, is attributed to a lowering of the lattice order. Moreover, the shoulder observed at 2θ = 3°, could also be indicating the beginning of a phase transformation [31]. Thus, the hydrothermal synthesis time has a considerable effect on the structural order of the samples. This effect was analyzed for the Si/Ni molar ratios of 20 and 60, evaluating the degree of structural ordering for each sample in comparison to a sample arbitrarily taken as reference with 100% of ordering (Si/Ni 60 or 20 and hydrothermal synthesis of 3 days) [32,33]. Thus, Fig. S1 (Supporting Information) shows the degree of structural ordering of the samples in function of hydrothermal treatment days. As it can be observed, the structural regularity was increased when the sample was hydrothermally treated. For both Si/Ni ratios (20 and 60), a hydrothermal treatment time of 3 days appears optimum to obtain the best structure. Then, a longer time appears to induce some disorder in the structure [34,35], probably associated with an incipient phase transformation [31,36,37]. In addition, it is notable that for Si/Ni = 20 samples the structural deterioration, caused for hydrothermal treatment days increasing, is more pronounced.

On the other hand, several works have already reported that the lattice parameter $a_0$ is affected by the introduction of different elements, causing an expansion of the mesoporous channels [25,33,38,39]. The substitution of $Si^{4+}$ by the $Ni^{2+}$ ions might distort the pore arrangement due to an increase in the bond distance. Therefore, the increment in the $a_0$ parameter and in the pore diameter (Table 1) with the increase in the hydrothermal synthesis days could evidence the Ni incorporation inside the framework. However, the Ni content determined by ICP (Table 1) was maximum (lowest Si/Ni molar ratio) for the samples hydrothermal synthesized for 3 days. An increment in the hydrothermal time leads to a lower Ni content, which could be attributed to a re-dissolution process favored by the hydrothermal treatment. Thus, a hydrothermal treatment time above 3 days could disturb the self-assembly process and induce to bond cleavages in the silica, leading to Ni re-dissolution and its remove in the washing water.

The high-angle XRD patterns of the calcined samples (Fig. S2, in Supporting Information) exhibit some very small peaks (2θ = 37, 43 and 63°) characteristic of NiO oxide, whose intensities decrease with the hydrothermal treatment days. This suggests that such species could be finely dispersed, inside the mesochannels as well as on the external surface [40]. It should be noted that the characteristic peaks of nickel oxide are very attenuated in terms of intensity in relation to the broad peak corresponding to MCM-41 amorphous silica (2θ = 23°). As it has already been reported [38] it is probable that for low metal contents, the clusters and oxide nanoparticles form inside the mesopores and when the metal loading exceeds some critical concentration, the nanoparticles are also nucleated on the external surface of the support. In contrast with these results, when mesoporous silica MCM-41 was modified with Ni by the impregnation method [26], we could observe larger NiO nanoparticles for samples with similar metal contents. Therefore, this method of direct incorporation leads to oxide species very finely dispersed on the support. Moreover, the hydrothermal treatment would lead to a higher stabilization of the Ni into the framework and lower segregation of oxides.

**Table 1**
Structure properties and chemical composition of the synthesized samples.

| Sample | Si/Ni [a] | Area ($m^2$/g) [b] | Ni content (wt. %) [c] | Si/Ni | $D_p$ (nm) [d] | $V_{TP}$ ($cm^3$/g) | $a_0$ (nm) [e] |
|---|---|---|---|---|---|---|---|
| Ni(20)0 | 20 | 845 | 3.4 | 27 | 3.5 | 0.70 | 4.21 |
| Ni(20)1 | 20 | 840 | – | – | 3,7 | 0.82 | 4.35 |
| Ni(20)3 | 20 | 855 | 6.6 | 13 | 3,8 | 0.83 | 4.52 |
| Ni(20)5 | 20 | – | – | – | – | – | 4.45 |
| Ni(20)7 | 20 | 522 | 2.9 | 23 | 3.9 | 0.48 | 4.19 |
| Ni(60)0 | 60 | 966 | 1.6 | 58 | 3.5 | 0.81 | 4.09 |
| Ni(60)1 | 60 | 875 | – | – | 3.7 | 0.80 | 4.40 |
| Ni(60)3 | 60 | 836 | 2.6 | 39 | 3.8 | 0.73 | 4.44 |
| Ni(60)5 | 60 | – | – | – | – | – | 4.51 |
| Ni(60)7 | 60 | 610 | 1.9 | 49 | 3.8 | 0.41 | 4.35 |

[a] In synthesis gel.
[b] Determined by BET.
[c] Determined method ICP.
[d] $N_2$ adsorption-desorption.
[e] $a_0 = (2/\sqrt{3})d_{100}$.

The $N_2$ adsorption–desorption isotherms and NLDFT pore size distribution (inset) for calcined samples are illustrated in Fig. 2a and b. All the samples exhibit type IV isotherms, typical of a well-defined mesoporous structure with an inflection at $p/p^0$ = 0.2–0.35, characteristic of capillary condensation inside the mesopores of the MCM-41 structure [41,42]. However, the adsorption capacity of all Si/Ni = 20 samples decreased in comparison with Si/Ni = 60 samples, probably due to the increased presence of clusters and/or small particles of metal oxides finely dispersed inside the channels as well as some nanoparticles on the external surface, which affects the pore structure and the textural properties of the materials. The results obtained from the isotherms are collected in Table 1. All of the materials show high area and pore volume, typical of MCM-41 materials.

It is important to note that the Ni(60)0 sample exhibits an pronounced hysteresis loop H4 by the IUPAC classification, with a sharp decrease of the desorption branch at $p/p^0$ = 0.45–0.5. This feature could be related to the presence of interconnected pores and a percolation effect, although the soft fall in the desorption branch at these $p/p^0$ values would permit discarding the presence of ink-bottle pores [43]. In addition, the shape of the hysteresis loop changes as the hydrothermal treatment increases, giving account for the formation of more uniform shape pores. However, for both Ni contents, the isotherms of the samples hydrothermal treated for more than 3 days show an important decrease in the adsorbed amount, which is in concordance with the decrease on the specific surface and the structural ordering (evidenced by XRD). Also, these samples present a lighter inflection at $p/p^0$ = 0.3–0.4, giving account for a broader pore size distribution.

On the other hand, the isotherms for both Si/Ni ratios present an increase in the adsorption branch at $p/p^0 \sim 0.9$, which is ascribed to structural defects and/or capillary condensation in secondary mesopores. The direct incorporation of the metal in the initial synthesis gel and subsequent hydrothermal treatment would be responsible of secondary mesoporosity generation. Díaz et al. [44] have reported that a change in the micellar size, due to the presence of metallic species in synthesis medium, might favor the change from cylindrical micelles to more complex aggregates. These aggregates would be responsible for the building-up of such secondary porosity. Thus, a great amount of metal in the synthesis medium may interfere with the formation of the micelles by changing its ionic strength, giving rise to these complex aggregates. Thus, this feature is more noteworthy for the Si/Ni = 20 samples, which have the higher Ni loading.

In addition, as it is observed in the pore size distribution (PSD) and cumulative pore volume calculated by NLDFT, all the samples present defined pore size, with a distribution of average pore size (Dp) of approximately 3.5 nm. It is noteworthy that with the increase of hydrothermal synthesis days, an increase in the average pore size is observed, which is in agreement with the heteroatom incorporation into the framework.

Measurements of transmission electron microscopy of the calcined materials were made in order to examine their structural regularity (See the Supporting Information, Fig. S3).

UV–Vis DRS spectroscopy is used to infer about the coordination

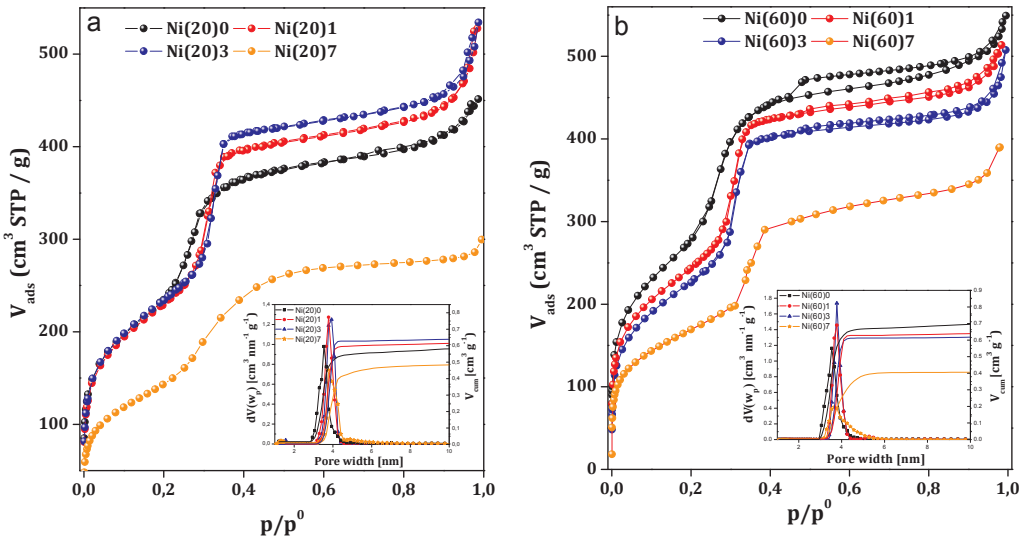


**Fig. 2.** Nitrogen adsorption-desorption isotherms of samples with Si/Ni molar ratios (a) 20 and (b) 60. Inset: NLDFT pore size distribution and cumulative pore volume of samples.

environment of different Ni species on the synthesized mesoporous samples. The spectra of the calcined and non-calcined samples with different hydrothermal treatment times are shown in Fig S4a and b (Supporting Information).

Temperature-programmed reduction (TPR) is an extremely sensitive technique that allows studying the reduction process of metallic species on the solid, in order to determine the number of these reducible species on the catalyst and the reduction temperature. It is known that the reduction of the metal oxide species depends on the particles size and the interaction of these with the support. The reduction takes place involving all the reducible species, but not all particles are exposed to hydrogen at the same time. Therefore, a decrease in the particle size of the metal oxide makes the reduction faster due to a higher surface/volume ratio, although these smaller particles can interact more intensely with the support and thus slow down the reduction. Therefore, the reducibility of the materials would be the result of the competition of these two factors. The TPR profiles of the catalysts prepared in this study with two different Si/Ni molar ratios (20 and 60) in the synthesis mixture are illustrated in Fig. 3. In the case of Ni(20) samples, these show a main peak at 923 K together with a shoulder about at 723 K. This broad band can indicate nickel species with different reducibility and interacting differently with the support, either dispersed on the surface or located inside the pores of the catalyst [45]. Besides, the samples with Si/Ni = 60 M ratio present different profiles. Thus, an intense and broad peak is observed for the Ni(60)0 at 673 K, whereas that other catalysts exhibit a main peak at 673 K with other maximum at higher temperatures (773–873 K). This fact suggests that the higher reduction temperatures could be due to the nickel incorporation into the mesoporous framework. Therefore, when the treatment days increase, a high presence of Ni species more hardly reducible is achieved. This feature is in concordance with the evidences from UV–Vis about on the higher isolated nickel incorporation (both onto inner surface and inside the mesoporous walls) with hydrothermal time increasing.

On the other hand, it is worth to note that the reduction process in the Ni(20) samples extends at a higher temperature, probably due to that highly dispersed species could be protected by the oxides coverage, which is in concordance with UV–Vis analysis and $N_2$ isotherms.

Infrared spectroscopy has been extensively used for the characterization of surface functional groups in solid catalysts (See the Supporting Information, Fig. S5).

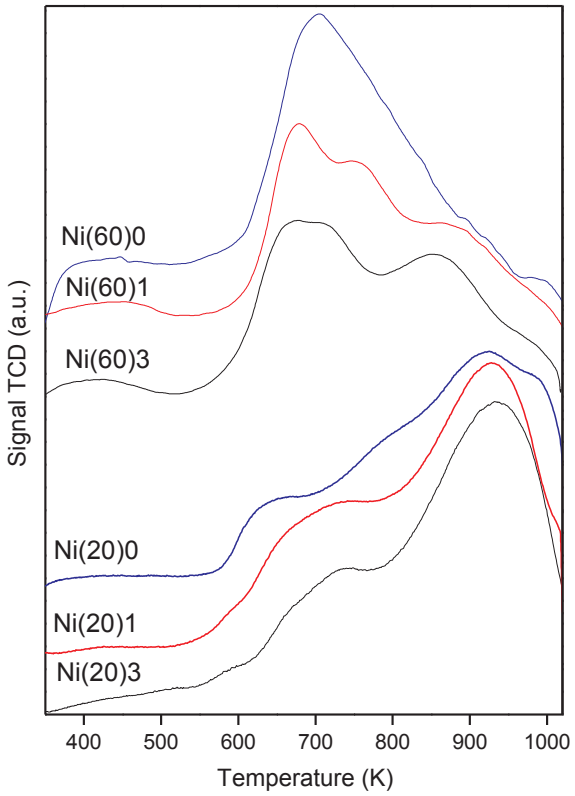


**Fig. 3.** TPR profiles of samples with Si/Ni molar ratios 20 and 60.

### 3.2. Energy and environmental applications

In order to study the hydrogen adsorption capacity at 77 K, calcined materials with good structural ordering and different nickel dispersion were selected. The Fig. 4 shows the adsorption excess isotherms of representative samples measured at 77 K and pressure up to 10 bar. All the isotherms are totally reversible. Furthermore, the shape of the excess isotherm at high pressures is mainly influenced by the equation of state of the adsorptive and, usually the isotherm will present a maximum, after which, the excess amount tends to diminish. The position of this point depends basically of the adsorbate-adsorbent interaction as well as on the thermodynamic state of the adsorptive [46]. In Fig. 4,

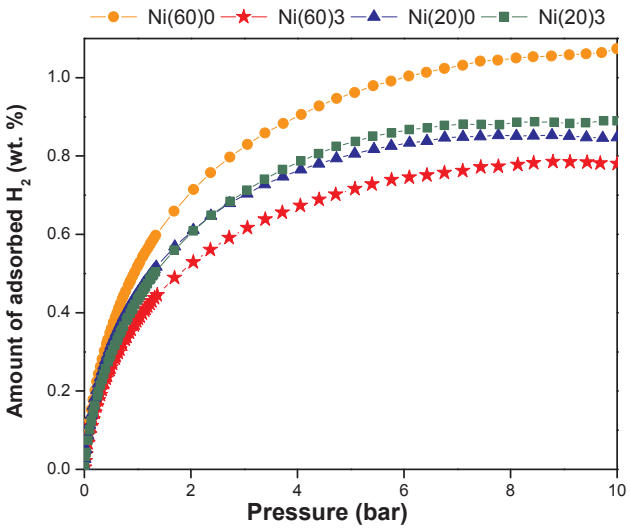


**Fig. 4.** $H_2$ adsorption-desorption isotherms of samples with Si/Ni molar ratios 20 and 60, measured at 77 K.

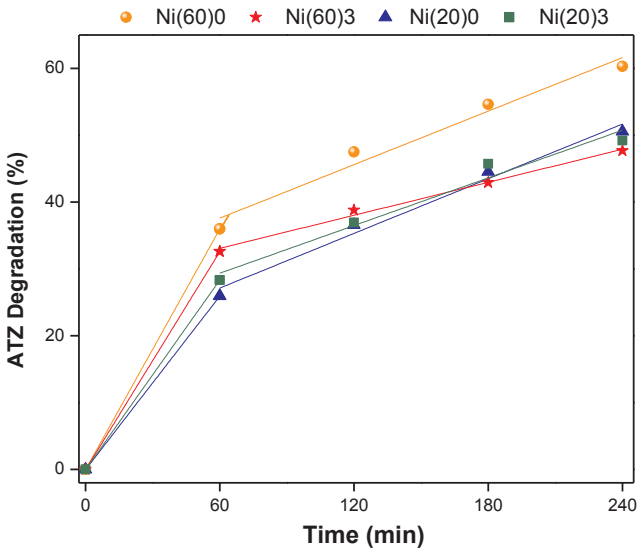


**Fig. 5.** % ATZ concentration as a function of time for the heterogeneous photo-Fenton reaction of synthesized samples with Si/Ni molar ratios 20 and 60.

this maximum was not observed for the calcined samples, due to that the maximum storage capacity at 10 bar has not been reached yet. This is important to take into account in the design of materials for hydrogen storage.

The Ni(60)0 sample shows the highest capacity of $H_2$ storage at 77 K, reaching a 1.1 wt.% near 10 bar. It is important to mention that this sample also presents the higher $S_{BET}$ parameter which would also be important in the $H_2$ adsorption at 77 K. In our previous reports [26,28], the Density Functional Theory calculations demonstrated that the sites responsible of the $H_2$ adsorption on $Ni/SiO_2$ system are Ni atoms with low coordination. Therefore, the nickel species dispersed on the MCM-41 support could be promoting the presence of hydrogen-favorable sites, responsible for the highest $H_2$ adsorption capacity at 77 K. Comparing the behavior of the Ni(60)0 sample with the sample with 3 hydrothermal treatment days, the decrease in the hydrogen storage capacity with the increase of the hydrothermal days could be probably associated with the incorporation of such Ni sites within the mesopore walls, which would decrease the accessibility of these sites towards hydrogen. It noteworthy that although with the hydrothermal treatment days the nickel isolated species proportion overcomes to that of the oxide, these species (incorporated in higher proportion inside the walls) would be less accessible. In addition, is noteworthy that a decrease in the $S_{BET}$ was observed with the increase of hydrothermal synthesis days, which is in agreement with the decreased in the $H_2$ adsorption.

On the other hand, when the nickel loading is increased, the samples with Si/Ni ratio of 20 show a minor adsorption capacity. This behavior may be probably due to a blocking effect of the adsorption sites by larger Ni oxides. Even an opposite behavior was found for the samples with Si/Ni = 20, the difference in the $H_2$ adsorbed amount between the Ni(20)0 y Ni(20)3 samples is slightly small, whereby it could be considered depreciable. The fact that these samples have the same behavior could be attributed to that besides their $S_{BET}$ are similar, the accessibility to active sites is diminished for both samples.

Thus, in our previous report [26,47], the hydrogen storage capacity of the pure MCM-41 was 0.88 wt.% around 5–6 bar, after which, the hydrogen uptake diminishes. Therefore, it is clear that the Ni containing mesoporous materials has a positive effect on the hydrogen sorption capacity.

On the other hand, the feasibility of the ATZ degradation by a heterogeneous photo-Fenton-like process with nickel modified mesoporous silica was investigated. Experiments were conducted under the best operating conditions for ATZ degradation reported by Benzaquén et al. [30].

The atrazine degradation using the calcined samples with both Si/metal ratios (Si/Ni = 20 and 60) and for a hydrothermal treatment time of 0 and 3 days, is presented in Fig. 5. As it can be observed, the activity reached a maximum for the sample with a Si/Ni = 60 ratio and hydrothermal treatment time of 0 days. Thereby, a decrease of the ATZ degradation is observed with the hydrothermal treatment days for Si/Ni = 60, probably due to the incorporation of the active species inside the pore walls. This is once again according to the behavior observed previously, whereby the catalytic activity of Ni(60)0 sample is due to the highly dispersed nickel species on the MCM-41, favouring the accessibility of the reactant molecules to the active site. Then, an increase of the Ni content (Si/Ni molar ratio = 20) did not introduce an atrazine conversion enhancement, leading to a lower reactant degradation. Besides, both samples (Ni(20)0 y Ni(20)3) presented similar catalytic activity. Such behavior would be probably due to a blocking of the active species protected by the covering with oxide species.

In addition, the Turnover Numbers (TON, defined as moles of atrazine degraded/moles of Ni) were calculated at the end of the catalytic reaction [48]. These values are shown in Table S2 (Supporting Information). It is can be seen, they steadily decrease with increasing metal content which would indicate that, much of the Ni is not effectively used during the catalytic photo-oxidation. This fact could be confirming a possible blocking of the Ni species responsible for the ATZ degradation.

Finally, in order to confirm the presence of dispersed Ni species on the support (sites responsible for the hydrogen adsorption and catalytic activity), the adsorption of pyridine coupled to IR spectroscopy was carried out for the calcined samples with initial Si/Ni molar ratio = 60. The pyridine is used as a probe molecule for qualitative and quantitative determination of both Brønsted and Lewis acid sites. In a previous report [26,28], we determined the presence of highly dispersed Ni species judging by the formation of adducts of pyridine-Lewis sites attributed to the interaction between Ni unoccupied molecular orbitals and pyridine.

Here, the IR spectra of pyridine adsorbed on the materials (Fig. 6) show the characteristic bands at 1597 and 1447 $cm^{-1}$, which correspond to hydrogen-bonded pyridine, since pyridine can form hydrogen bonds with the silanol groups present in the structure. However, it is necessary to clarify that this last band at 1447 $cm^{-1}$ appears overlapped with the band at 1445–1455 $cm^{-1}$ corresponding to the Lewis acidity [32–34]. It is noteworthy that this acidity decreased when the

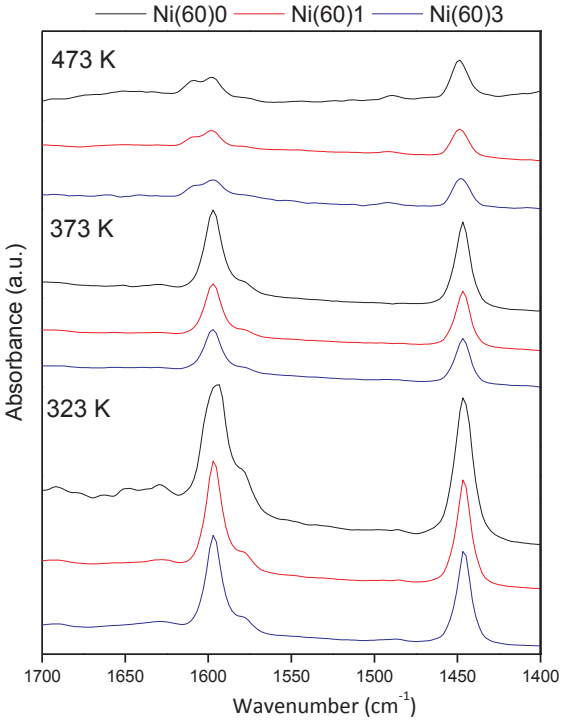


**Fig. 6.** FT-IR spectra of pyridine adsorbed on the synthesized samples with Si/Ni molar ratio 60. Desorption at 323 K, 373 K and 473 K.

synthesis time is about 3 days. This behavior may be probably assigned to the decrease of the Lewis acid sites over the pore walls due to the incorporation of nickel into the silica framework.

Then, the pyridine thermodesorption at 323, 373 and 473 K for an hour allowed us to infer about the strength of Lewis acid sites. Thus, the intensities of all bands decreased when the temperature reached 473 K under vacuum. Such feature indicates that the Lewis sites are strong enough to retain the pyridine molecules until 473 K.

Therefore, the results of pyridine chemisorption followed by IR spectroscopy for these samples (along with other characterizations techniques) confirmed the presence of highly dispersed Ni species. These pyridine-Lewis adducts decrease with increasing hydrothermal synthesis days due to the Ni incorporation inside the structure. Whereby, these sites would be the sites responsible for the $H_2$ adsorption capacity and ATZ degradation by the heterogeneous photo-Fenton process.

## 4. Conclusion

Nickel modified mesoporous silica with MCM-41 structure were prepared by the direct hydrothermal synthesis method. The effect of Ni loading and the hydrothermal treatment days on the textural, structural, adsorption and catalytic properties of the materials was investigated. The samples presented well-ordered hexagonal mesostructure, however the structural regularity appears to be slightly decreased for 5 and 7 hydrothermal treatment days. The increase of the hydrothermal treatment leads to lower oxide segregation and favours the Ni incorporation inside mesoporous framework. Thus, combined characterization results indicate that the synthesis time has an important influence on the textural, structural and chemical properties of the nickel modified mesoporous silica. Likewise, the increase in the Si/Ni molar ratio leads to higher presence of nickel oxide.

Hydrogen adsorption capacity of Ni-containing mesoporous materials modified with nickel was measured at 77 K up to 10 bar. The results demonstrated that the sample with a molar ratio Si/Ni = 60 and without hydrothermal treatment presented the highest hydrogen adsorption, probably due to their high $S_{BET}$ and the accessibility to active nickel species highly dispersed on the support. Thus, although the hydrothermal time leads to the isolated nickel species incorporation into the framework, also could enhance their introduction inside the mesoporous walls decreasing their accessibility. When the Si/Ni molar ratio increase, the accessibility to active sites is diminished due to blocking of the active species protected by the covering with oxide species.

Besides, the mesostructured nickel-containing catalysts have been successfully proved in Atrazine degradation by the heterogeneous photo-Fenton-like process in aqueous solutions. As a result of this, the sample with nickel loading of 1.6 wt.% (Ni(60)0) allowed to reach values of the pollutant degradation of about 60.3%.

In conclusion, the nickel containing mesoporous silica presents the option of developing materials versatile and efficient to be employed in energy and environmental applications.

## Funding

This study was funded by Universidad Tecnológica Nacional (UTN-FRC), Universidad Nacional de Córdoba (UNC) and Consejo Nacional de Investigaciones Científicas (CONICET).

## Conflict of interest

The authors declare that they have no conflict of interest.

## Appendix A. Supplementary material

Supplementary data to this article can be found online at https://doi.org/10.1016/j.cplett.2018.10.036.

## References

[1] International Energy Agency, Technology Roadmap: Hydrogen and Fuel Cells. < http://www.iea.org/publications/freepublications/publication/technology-roadmap-hydrogen-and-fuel-cells.html > Accessed 26 March 2018.
[2] G. Nicoletti, The hydrogen option for energy: a review of technical, environmental and economic aspects, Int. J. Hydrogen Energy 20 (1995) 759.
[3] C. Read, G. Thomas, C. Ordaz, S. Satyapal, U.S. department of energy's system targets for on-board vehicular hydrogen storage, Mater. Matters 2 (2007) 3.
[4] A. Zuttel, Hydrogen storage methods, Mater. Today 6 (2003) 24.
[5] U.S. Department of Energy Hydrogen Program: < www.hydrogen.energy.gov > .
[6] W.Q. Fan, T. Yanase, H. Morinaga, S. Ondo, T. Okabe, M. Nomura, T. Komatsu, K.I. Morohashi, T.B. Hayes, R. Takayanag, H. Nawata, Atrazine-induced aromatase expression is sf-1 dependent: implications for endocrine disruption in wildlife and reproductive cancers in humans, Environ. Health Persp. 727 (2007) 115.
[7] S. Luciane, C. Attilio, A.R.S. Geslaine, D.C.G.S. Rita, New aspects on atrazine biodegradation, Braz. Arch. Biol. Techn. 53 (2010) 487.
[8] L. Erickson, K.H. Lee, Degradation of atrazine and related s-triazine, CRC Crit. Rev. Env. Contr. 19 (1989) 1.
[9] D.A. Belluck, S.L. Benjamin, T. Dawson, Groundwater contamination by atrazine and its metabolites: risk assessment, policy and legal implication, Pesticide Transformation Products, American Chemical Society, Washington, DC, 1991, pp. 254–273.
[10] M.A. Quiroz, E.R. Bandala, C.A. Martínez-Huitle, Pesticies-Formulations, Effect, Fate, InTech Press, 2011.
[11] T.B. Benzaquén, M.A. Islaa, O.M. Alfano, Combined chemical oxidation and biological processes for herbicide degradation, Chem. Technol. Biotechnol. 90 (2015) 459.
[12] W. Chu, K.H. Chan, C.Y. Kwan, K.Y. Choi, Degradation of atrazine by modified stepwise-Fenton's processes, Chemosphere 67 (2007) 755.
[13] S.-Q. Liu, B. Xiao, L.-R. Feng, S.-S. Zhou, Z.-G. Chen, C.-B. Liu, F. Chen, Z.-Y. Wu, N. Xu, W.-C. Oh, Z.-D. Meng, Graphene oxide enhances the Fenton-like photocatalytic activity of nickel ferrite for degradation of dyes under visible light irradiation, Carbon 64 (2013) 197.
[14] S.-Q. Liu, L.-R. Feng, N. Xu, Z.-G. Chen, X.-M. Wang, Magnetic nickel ferrite as a heterogeneous photo-fenton catalyst for the degradation of rhodamine b in the presence of oxalic acid, Chem. Eng. J. 203 (2012) 432.
[15] R. Sharma, S. Bansal, S. Singhal, RSC Adv. 5 (2015) 6006.
[16] O.S.N. Sum, J. Feng, X. Hu, P.L. Yue, Tailoring the photo-Fenton activity of spinel ferrites (MFe2O4) by incorporating different cations (M = Cu, Zn, Ni and Co) in the structure, Top. Catal. 33 (2005) 233.
[17] J. Herney-Ramirez, Miguel A. Vicente, L.M. Madeira, Heterogeneous photo-fenton oxidation with pillared clay-based catalysts for wastewater treatment: a review,

Appl. Catal. B: Environ. 98 (2010) 10.
[18] C.T. Kresge, M.E. Leonowicz, W.J. Roth, J.C. Vartuli, J.S. Beck, Ordered mesoporous molecular sieves synthesized by a liquid-crystal template mechanism, Nature 359 (1992) 710.
[19] S. Zheng, L. Gao, Synthesis and characterization of Pt, Au or Pd clusters deposited titania-modified mesoporous silicate MCM-41, Mater. Chem. Phys. 78 (2003) 512.
[20] H. Arbag, S. Yasyerli, N. Yasyerli, G. Dogu, Activity and stability enhancement of Ni-MCM-41 catalysts by Rh incorporation for hydrogen from dry reforming of methane, Int. J. Hydrogen Energy 35 (2010) 2296.
[21] N.H.H. Abu Bakar, M.M. Bettahar, M. Abu Bakar, S. Monteverdi, J. Ismail, Low temperature activation of Pt/Ni supported MCM-41 catalysts for hydrogenation of benzene, J. Mol. Catal. A: Chem 333 (2010) 11.
[22] M. Abdollahi-Alibeik, A. Moaddelia, New J. Chem. 39 (2015) 2116.
[23] N. Bouazizi, R. Ouargli, S. Nousir, R. Ben Slama, A. Azzouz, Properties of SBA-15 modified by iron nanoparticles as potential hydrogen adsorbents and sensors, J. Phys. Chem. Solids 77 (2015) 172.
[24] L. Mercier, T.J. Pinnavaia, Heavy metal ion adsorbents formed by the grafting of a thiol functionality to mesoporous silica molecular sieves: factors affecting Hg (II) uptake, Adv. Mater. 9 (1997) 500.
[25] S. Park, S.Y. Lee, A study on hydrogen-storage behaviors of nickel-loaded mesoporous MCM-41, J. Colloid Interf. Sci. 346 (2010) 194.
[26] P.M. Carraro, V.R. Elías, A.A. García Blanco, K. Sapag, S. Moreno, M.I. Oliva, G.A. Eimer, Synthesis and multi-technique characterization of nickel loaded MCM-41 as potential hydrogen-storage materials, Micropor. Mesopor. Mater. 191 (2014) 103.
[27] Y. Yamamoto, N. Nawa, S. Nishimoto, Y. Kameshima, M. Matsuda, M. Miyake, Temperature dependence of hydrogen adsorption properties of nickel-doped mesoporous silica, Int. J. Hydrogen Energy 36 (2011) 5739–5743.
[28] P.M. Carraro, A.A. García Blanco, F.A. Soria, G. Lener, K. Sapag, G.A. Eimer, M.I. Oliva, Understanding the role of nickel on the hydrogen storage capacity of Ni/MCM-41 materials, Micropor. Mesopor. Mater. 231 (2016) 31.
[29] A.O. Allen, J.A. Hochanadel, J.A. Ghormley, T.W. Davis, Decomposition of water and aqueous solutions under mixed fast neutron and γ-radiation, J. Phys. Chem. 56 (1952) 575.
[30] T.B. Benzaquén, N.I. Cuello, O.M. Alfano, G.A. Eimer, Degradation of Atrazine over a heterogeneous photo-fenton process with iron modified MCM-41 materials, Catal. Today 296 (2017) 51.
[31] K.W.K. Gallis, C.C.C. Landry, Synthesis of MCM-48 by a phase transformation process, Chem. Mater. 9 (1997) 2035.
[32] V.R. Elías, M. Crivello, E.R. Herrero, S.G. Casuscelli, G.A. Eimer, Synthesis of titanium-containing mesoporous silicas as catalysts for cyclohexene epoxidation, Ind. Eng. Chem. Res 48 (2009) 9076.
[33] G.A. Eimer, C.M. Chanquia, K. Sapag, E.R. Herrero, The role of different parameters of synthesis in the final structure of Ti-containing mesoporous materials, Micropor. Mesopor. Mater. 116 (2008) 670.
[34] G.A. Eimer, S.G. Casuscelli, C.M. Chanquia, E. Crivello, E.R. Herrero, The influence of Ti-loading on the acid behavior and on the catalytic efficiency of mesoporous Ti-MCM-41 molecular sieves, Catal. Today 133–135 (2008) 639.
[35] E.G. Vaschetto, G.A. Monti, E.R. Herrero, S.G. Casuscelli, G.A. Eimer, Influence of the synthesis conditions on the physicochemical properties and acidity of Al-MCM-41 as catalysts for the cyclohexanone oxime rearrangement, Appl. Catal. A Gen. 453 (2013) 391.
[36] C.C. Landry, S.H. Tolbert, K.W. Gallis, A. Monnier, G.D. Stucky, P. Norby, J.C. Hanson, Phase transformations in mesostructured silica/surfactant composites. Mechanisms for change and applications to materials synthesis, Chem. Mater. 13 (2001) 1600.
[37] M. Selvaraj, A. Pandurangan, K.S. Seshadri, P.K. Sinha, K.B. Lal, Comparison of mesoporous Al-MCM-41 molecular sieves in the production of p-cymene for isopropylation of toluene, Catal. A 186 (2002) 173.
[38] N. Cuello, V. Elías, S. Urreta, M. Oliva, G. Eimer, Microstructure and magnetic properties of iron modified mesoporous silica obtained by one step direct synthesis, Mater. Res. Bull. 48 (2013) 3559.
[39] H.T. Gomes, P. Selvam, S.E. Dapurkar, J.L. Figueiredo, J.L. Faria, Transition metal (Cu, Cr, and V) modified MCM-41 for the catalytic wet air oxidation of aniline, Micropor. Mesopor. Mater. 86 (2005) 287.
[40] D.J. Lensveld, J. Gerbrand Mesu, A. Jos van Dillen, K.P. de Jong, Synthesis and characterisation of MCM-41 supported nickel oxide catalysts, Micropor. Mesopor. Mater. 44–45 (2001) 401.
[41] A. Corma, From microporous to mesoporous molecular sieve materials and their use in catalysis, Chem. Rev. 97 (1997) 2373.
[42] P.I. Ravikovitch, A.V. Neimark, Characterization of micro- and mesoporosity in SBA-15 materials from adsorption data by the NLDFT method, J. Phys. Chem. B 105 (2001) 6817.
[43] F. Rouquerol, J. Rouquerol, K. Sing, Adsorption by Powders and Porous Solids. Principles, Methodology and Applications, Academic Press, New York, 1999.
[44] I. Díaz, J. Pérez-Pariente, Synthesis of spongelike functionalized MCM-41 materials from gels containing amino acids, Chem. Mater. 14 (2002) 4641.
[45] T. Lehmann, T. Wolff, C. Hamel, P. Veit, B. Garke, A. Seidel-Morgenstern, Physicochemical characterization of Ni/MCM-41 synthesized by a template ion exchange approach, Micropor. Mesopor. Mater. 151 (2012) 113.
[46] M. Bastos-Neto, C. Patzschke, M. Lange, J. Möllmer, A. Möller, S. Fichtner, C. Schrage, D. Lässig, J. Lincke, R. Staudt, H. Krautscheid, R. Gläser, Assessment of hydrogen storage by physisorption in porous materials, Energy Environ. Sci. 5 (2012) 8294.
[47] P.M. Carraro, K. Sapag, M.I. Oliva, G.A. Eimer, Comparative study of hydrogen storage on metal doped mesoporous materials, Chem. Phys. Lett. 701 (2018) 93.
[48] G.A. Eimer, S.G. Casuscelli, G.E. Ghione, M.E. Crivello, E.R. Herrero, Synthesis, characterization and selective oxidation properties of Ti-containing mesoporous catalysts, Appl. Catal. A Gen. 298 (2006) 232.